# First-principles calculations of the structural and dynamic properties, and the equation of state of crystalline iodine oxides $I_2O_4$, $I_2O_5$, and $I_2O_6$

Zhongqing Wu, Rajiv K. Kalia, Aiichiro Nakano, and Priya Vashishta[a)]
*Collaboratory for Advanced Computing and Simulations, Department of Chemical Engineering & Materials Science, Department of Physics & Astronomy, and Department of Computer Science, University of Southern California, Los Angeles, California 90089-0242, USA*

(Received 29 November 2010; accepted 22 April 2011; published online 23 May 2011)

The structural and dynamical correlations, and the equation of state of crystalline $I_2O_4$, $I_2O_5$, and $I_2O_6$ are investigated by first-principles calculations based on the density functional theory (DFT). The lattice dynamics results reveal distinctive features in the phonon density of states among the three crystals. The frequencies of the stretch modes in $I_2O_4$ and $I_2O_5$ are clearly separated from those of the other (e.g., bending) modes by a gap, with all stretch modes above the gap. In contrast, the gap in $I_2O_6$ separates the highest-frequency stretch modes with other stretch modes, and there is no gap between the stretch and the other modes in $I_2O_6$. The motion of iodine atoms is involved in all vibrational modes in $I_2O_5$, but only in low-frequency lattice modes in $I_2O_6$. In $I_2O_4$, iodine atoms are involved in modes with frequency below 700 $cm^{-1}$. Van der Waals correction within our DFT calculations is found to reduce the overestimation of the equilibrium volume, with its effect on structure similar to the pressure effect. Namely, both effects significantly decrease the inter-molecular distances, while slightly increasing the bond lengths within the molecules. This causes the frequencies of some vibrational modes to decrease with pressure, resulting in negative "modes Grüneisen parameters" for those modes. Thermodynamic properties, derived from the equation of state, of crystalline $I_2O_4$, $I_2O_5$, and $I_2O_6$ are discussed within the quasi-harmonic approximation. © *2011 American Institute of Physics*. [doi:10.1063/1.3590278]

## I. INTRODUCTION

Iodine oxides, $I_2O_4$, $I_2O_5$, and $I_2O_6$, are important inorganic compounds for a number of scientific, technological, and environmental issues, and they have been studied since the early days of the chemistry. For example, they are involved in ozone depletion and are used in the synthesis of various compounds. Recently, formation of iodine-containing ultrafine particles with a composition of $I_2O_5$ (Ref. 1) has been observed in costal marine environments,[2–7] and their impacts on the global climate have been widely discussed.[2,5,7] In addition, positive halogen compounds such as iodine oxides are known to destroy chemical and biological agents efficiently, with potential defense applications.[8] In such "agent defeat" applications, the knowledge of thermo-mechanical properties of iodine oxides at high temperatures and pressures is indispensable for understanding the nature and fate of these oxidants in explosion and combustion[9–11] and for identifying the active species formed under such conditions.

Although iodine oxides have been studied over 200 years, most investigations have focused on their non-solid phases, and the knowledge about iodine oxide crystals is still limited. Among all iodine oxides, $I_2O_4$, $I_2O_5$, and $I_2O_6$ can exist in crystal forms. Their experimental crystal structures including the atomic positions are available.[12–15] Raman and infrared experiments have been carried out to study the vibrational properties of $I_2O_4$ and $I_2O_5$ crystals.[16–20] But to the best of our knowledge, vibrational properties of crystalline $I_2O_6$ are not available in literature. Thermodynamic data such as thermal expansion, heat capacity, and bulk modulus are not known for all three crystals. Due to various difficulties such as crystal preparation, experimental determination of thermodynamic properties of the iodine oxide crystals is a challenge, and thus it is important to determine them theoretically.[21]

Though gas-phase properties of iodine oxides have been investigated using first principles methods,[22–26] no density functional theory (DFT) calculation on their crystalline phases has been reported. DFT calculation can provide vibrational properties using the density functional perturbation theory (DFPT),[27] and can determine thermodynamic properties within the quasi-harmonic approximation.[27–33] Here we use DFT calculation to calculate structural, vibrational, and thermodynamic properties of the three iodine oxides $I_2O_4$, $I_2O_5$, and $I_2O_6$, in their crystalline state. In our DFT calculations, van der Waals (vdW) correction is included using an empirical method proposed by Grimme.[34,35]

## II. METHOD

Computations are performed using the Quantum ESPRESSO, a DFT software package based on the plane-wave basis and pseudopotentials.[36] DFT, developed by Hohenberg and Kohn[37] and Kohn and Sham,[38] is the most popular first principle method on quantum mechanical calculations. It is an exact theory of the ground state and reduces the interacting many-electrons problem to a simple single-electron problem. DFT states that the ground state

a)Author to whom correspondence should be addressed. Electronic mail: priyav@usc.edu.

 

total energy of a system is unique functional of the charge density $n(\mathbf{r})$

$$E[n(\mathbf{r})] = F[n(\mathbf{r})] + \int V_{ion}(\mathbf{r})n(\mathbf{r})d\mathbf{r}. \quad (1)$$

Functional $F[n]$ contains the electronic kinetic energy and all the electron-electron interactions and is independent of the external potential, which is usually the Coulomb potential $V_{ion}$ due to ions (or nuclei) plus possible external field. The minimum value of the total energy functional is the ground state energy of the system at the ground state density.

A key to the application of DFT in handling the interacting electron gas was given by Kohn and Sham[38] by splitting up the kinetic energy of a system of interacting electrons into the kinetic energy of non-interacting electrons plus some remainder which can be conveniently incorporated into the exchange-correlation energy. The functional $F[n]$ can be written as

$$F[n(\mathbf{r})] = T[n(\mathbf{r})] + E_H[n(\mathbf{r})] + E_{XC}[n(\mathbf{r})]. \quad (2)$$

The explicit forms of kinetic energy, $T$, and Hartree energy, $E_H$, to the charge density are already known. The last term, $E_{XC}$, is the exchange-correlation energy and contains all the many-body effects in an interacting system. However the explicit forms for $E_{XC}$ and charge density is unknown except the simple case of the uniform electron gas. The charge density in real materials is not uniform, so the exchange-correlation functional cannot be calculated precisely. The local density approximation (LDA) replaces the exchange-correlation potential at each point $\mathbf{r}$ by that of a homogeneous electron gas with a density equal to the local density at point $\mathbf{r}$. The LDA works remarkably well for most of solid state materials but usually not well for molecules. Attempts to improve LDA through consideration of nonlocal corrections have met with some success. The generalized gradient approximation (GGA) is a marked improvement over LDA in the case of molecules. In this calculation, GGA with the Perdew-Burke-Ernzerhof (PBE)[39] scheme is adopted.

When the electron wave function is expanded using the plane wave basis, the pseudopotential method is required to reduce the computation workload. The core states participate little in bonding but require much higher plane-wave cutoff energy than valence states because of rapidly varying charge density of the core states. In pseudopotential method, the strong potential due to the nucleus and core electron is replaced by a weaker, more slowly varying potential with the same scattering properties (the pseudopotential). This approach speeds up calculations substantially because (1) only valence electrons are treated explicitly and (2) the pseudocharge density and potential vary much more slowly in space, which reduce the plane-wave cutoff energy significantly. The pseudopotentials for iodine and oxygen are generated by the method of Troullier and Martins.[40] The plane-wave cutoff energy is 70 Ry, and Brillouin-zone summations over electronic states are performed over 4 × 4× 4 k mesh with (1/2,1/2,1/2) shift.

The conventional DFT method summarized above has been found inadequate in treating vdW interactions between molecules in various solids such as energetic molecular crystals.[34,35,41] Here, we use an empirical method proposed by Grimme[34,35] to incorporate the vdW correction. The empirical dispersion correction is given by

$$E_{\text{disp}} = -s_6 \sum_{i<j} \frac{C_{ij}}{R_{ij}^6} f_{\text{damp}}(R_{ij}), \quad (3)$$

where $C_{ij}$ and $R_{ij}$ are the dispersion coefficient and interatomic distance between the $i$th and $j$th atoms, and $s_6$ is a global scaling factor. A damping function, $f_{\text{damp}}$, is introduced to ensure that the dispersion correction is negligible at small $R_{ij}$. All parameters except for $s_6$ are taken from the original literature.[34,35] We have modified $s_6$ from the original value, 0.75, proposed by Grimme for GGA, so as to reproduce the experimental equilibrium volume for crystalline iodine oxides $I_2O_4$, $I_2O_5$, and $I_2O_6$ at room temperature.

Structural optimization is achieved using the damped variable-cell-shape molecular-dynamics method[42] with and without the vdW correction. For each fully optimized structure, dynamical matrices are computed on a 2 × 2 × 2 q mesh using the DFPT,[27] further incorporating the vdW contribution, which are then interpolated on a regular 6 × 6 × 6 q mesh to obtain the vibrational density of state.

The vibrational modes are obtained by diagonalizing the dynamical matrices. The type of each vibrational mode (e.g., stretching, bending, rocking, wagging, as well as lattice translation and libration) is identified by visualizing the motions of one molecule in the crystalline unit cell. The motions of the other molecules can be derived based on the crystal symmetry. The visualization was performed with the Molden-4.7 software.

The Helmholtz free energy in the quasi-harmonic approximation is given by

$$F(V,T) = U_0(V) + \frac{1}{2}\sum_{q,j} \hbar\varpi_j(q,V) + k_B T \times \sum_{q,j} \ln\{1 - \exp[-\hbar\varpi_j(q,V)/k_B T]\}, \quad (4)$$

where the first, second, and third terms are the static internal energy, zero point energy, and vibrational energy contributions, respectively. The summation is performed on a 6 × 6 × 6 regular q mesh in the first Brillouin zone. The calculated Helmholtz free energy versus volume is fitted by an isothermal third-order finite strain equation of state (EOS). The resulting pressure-volume relation is described by a third-order Birch-Murnaghan EOS.[43]

## III. RESULTS

### A. Structure properties

$I_2O_4$ and $I_2O_5$ crystals have the same monoclinic structure and space group $P2_{1/c}$ with four molecules in the unit cell, whereas $I_2O_6$ crystal has the triclinic structure and belongs to space group $P\bar{1}$ with two molecules in the unit cell.

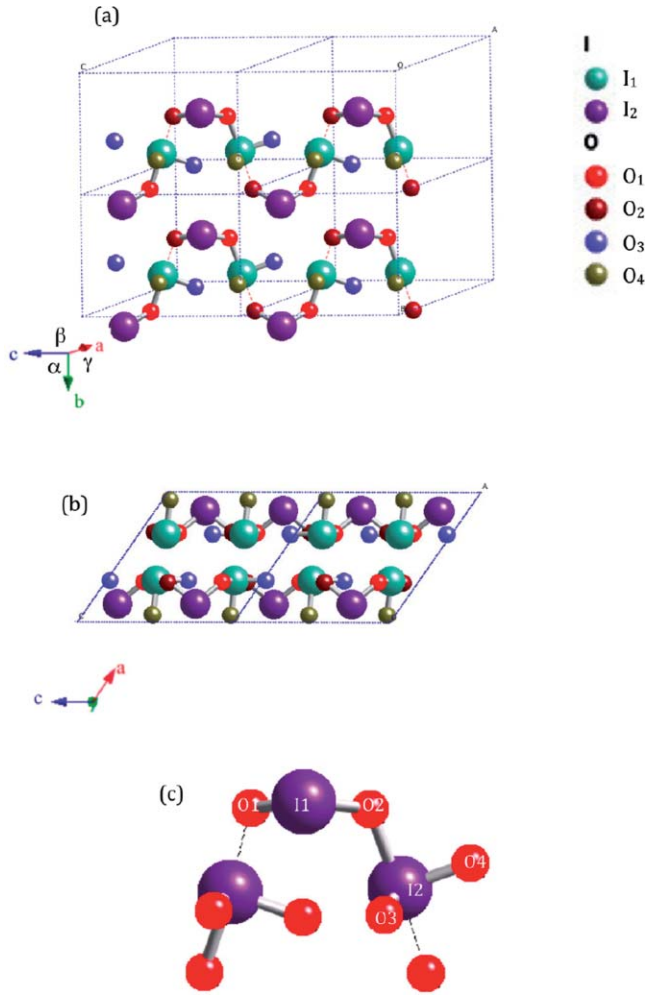


FIG. 1. The crystal structure of $I_2O_4$. (a) $I_2O_4$ molecules are connected by weaker inter-molecular bonds, which are shown by broken lines, to form a one-dimension chain. To clearly show the chain structure, we only show half of the atoms per unit cell, namely, we omit the atoms with $x > 0.5$, where $x$ is coefficient for basic vector along [100]. (b) The crystal structure projected along [010]. (c) $I_2O_4$ molecule with atom indices.

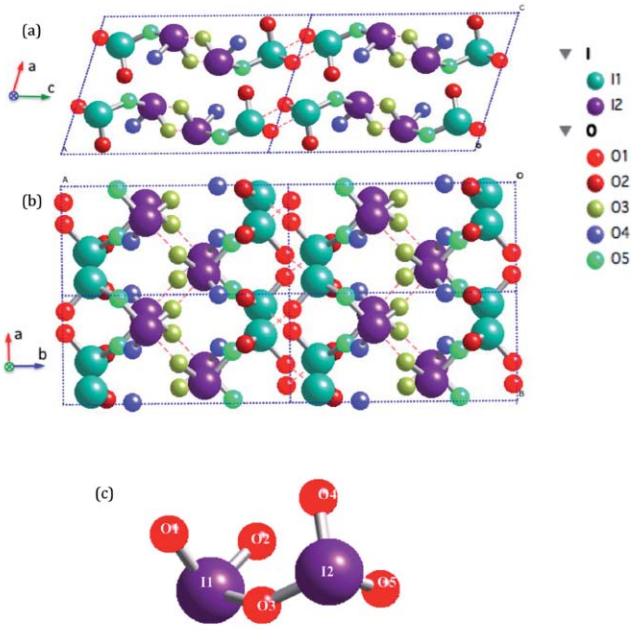


FIG. 2. The crystal structure of $I_2O_5$ projected along [010] (a) and along [001] (b). (c) $I_2O_5$ molecule with atom indices.

Figures 1–3 show the crystal structures of $I_2O_4$, $I_2O_5$, and $I_2O_6$, respectively.

The values for the lattice constants and atomic positions of the three materials $I_2O_4$, $I_2O_5$, and $I_2O_6$ are listed in Tables I and II. For all the crystals, it is obvious that the discrepancy between the experimental and calculated results without vdW correction is prominent along some directions. The anisotropy of vdW interaction is understood from the crystal structure as follows: The molecules in $I_2O_4$ crystal form a chain along the $c$ direction as shown in the Fig. 1. These chains are stacked in parallel along the $b$ direction, which results in large vdW interaction in the $b$ direction. The molecules in $I_2O_5$ crystal form a two-dimensional network in the $ab$ plane. We thus expect strong vdW interaction between different planes, i.e., along the $c$ direction, see Fig. 2. Also, $I_2O_5$ molecules are aligned mainly along the $a$ direction, which leads to anisotropic vdW interaction within the $ab$ plane. The molecules in $I_2O_6$ crystal lie in the $bc$ plane and are close to each other, see Fig. 3. Therefore, vdW interaction is small in the $bc$ plane compared to the out-of-plane interactions. Furthermore, since the molecules are aligned close to the [011] direction, the vdW interaction is similar along the $b$ and $c$ directions.

The equilibrium volumes calculated without vdW correction are far larger than the experimental volumes, i.e., by 7.9%, 9.9%, and 11.7%, respectively, for $I_2O_4$, $I_2O_5$, and $I_2O_6$. Such discrepancy in volume is common in molecular

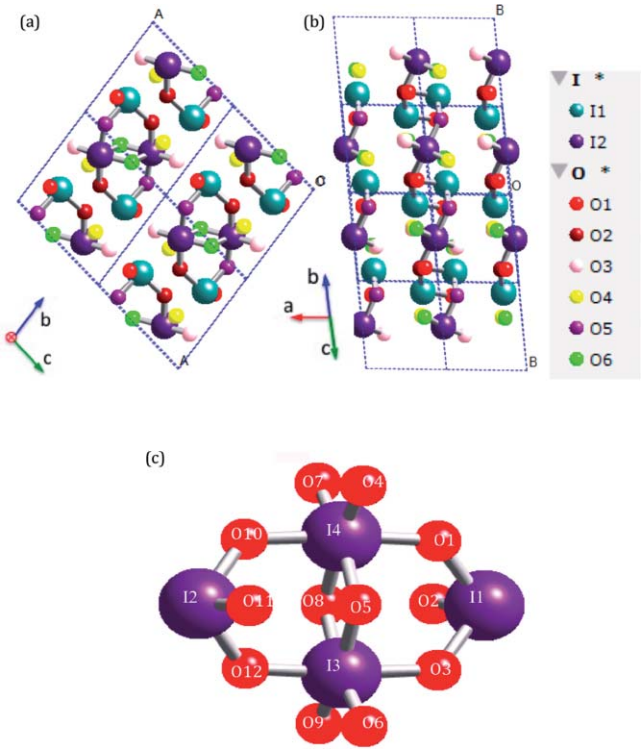


FIG. 3. The crystal structure of $I_2O_6$ projected along [100] (a) and along [011] (b). (c) Molecule $I_4O_{12}$ with atom index.

TABLE I. Lattice parameters and volume of crystalline $I_2O_4$, $I_2O_5$, $I_2O_6$ at 0 GPa. The lattice axes ($a$, $b$, $c$) of the crystalline unit cell and the angels between them ($\alpha$, $\beta$, $\gamma$) are defined in Fig. 1(a). The numbers in parentheses denote the deviation from the experimental data.

| | $a$ (Å) | $b$(Å) | $c$(Å) | $\alpha$ | $\beta$ | $\gamma$ | $V$(Å$^3$) | |
|---|---|---|---|---|---|---|---|---|
| $I_2O_4$ | 8.600 (1.3%) | 7.059 (5.4%) | 8.214 (1.4%) | | 122.63 (−1.7%) | | 419.97 (7.9%) | No vdW |
| | 8.369 (−1.3%) | 6.790 (1.4%) | 8.108 (−2.7%) | | 123.79 (−0.7%) | | 382.88 (−1.6%) | $s_6 = 0.75$[a] |
| | 8.483 | 6.696 | 8.33 | | 124.69 | | 389.15 | Exp.[b] |
| $I_2O_5$ | 11.116 (0.7%) | 5.265 (4.0%) | 8.525 (4.8%) | | 106.93 (−0.2%) | | 477.3 (9.9%) | No vdW |
| | 10.962 (−0.7%) | 5.075 (0.2%) | 8.131 (0.0%) | | 107.70 (0.5%) | | 430.92 (−0.8%) | $s_6 = 0.75$[a] |
| | 10.937 (−0.9%) | 5.052 (−0.2%) | 8.100 (−0.4%) | | 107.75 (0.5%) | | 426.3 (−1.9%) | $s_6 = 1.0$[a] |
| | 11.036 | 5.063 | 8.135 | | 107.18 | | 434.4 | Exp.[c] |
| $I_2O_6$ | 5.402 (7.3%) | 6.910 (2.5%) | 6.863 (1%) | 98.96 (1.7) | 95.16 (−1.3%) | 105.01 (−0.3%) | 242.1 (11.7%) | No vdW |
| | 5.064 (1.2%) | 6.894 (2.3%) | 6.846 (0.7%) | 97.79 (0.5%) | 96.56 (0.1%) | 105.40 (0.0%) | 225.4 (4.0%) | $s_6 = 0.75$[a] |
| | 4.883 (−2.3%) | 6.840 (1.5%) | 6.798 (0%) | 97.179 (−0.1%) | 98.23 (1.8%) | 105.07 (−0.3%) | 213.8 (−1.4%) | $s_6 = 2.0$[a] |
| | 5.006 | 6.741 | 6.795 | 97.31 | 96.45 | 105.36 | 216.8 | Exp.[d] |

[a]With van der Waals correction. The value of $s_6$, global scaling factor, in Eq. (3) is suggested to be 0.75 for GGA by Grimme.
[b]Reference 12.
[c]Reference 14.
[d]Reference 13.

crystals, and has been attributed to the inadequacy of the exchange-correlation functional in dealing with the vdW interaction. The vdW correction greatly reduces the volume difference between the experimental and calculated values to –1.6%, –0.8%, and 4.0%, respectively, for $I_2O_4$, $I_2O_5$, and $I_2O_6$.

Noting that the vibrational contribution to the volume usually increases the volume by about 2% (Refs. 29–32) at room temperature, the volume difference between calculation and experiment at ambient condition is still large for $I_2O_6$. In order to obtain a good equation-of-state for crystalline $I_2O_4$, $I_2O_5$, and $I_2O_6$, we modify the $s_6$ in Eq. (3) so as to reproduce the experimental equilibrium volume at room temperature. The corresponding $s_6$ values for the three crystals are listed in Table I. For $I_2O_4$, we do not need to modify the original $s_6$, since the calculated volume including the vdW correction and vibrational contribution agrees quite well with the experimental volume to within 0.3%. For $I_2O_5$, we increase $s_6$

TABLE II. Atomic positional parameters of crystalline $I_2O_4$, $I_2O_5$, $I_2O_6$ at 0 GPa.

| | | $I_2O_4$ | | | $I_2O_5$ | | | $I_2O_6$ | | |
|---|---|---|---|---|---|---|---|---|---|---|
| | | x | Y | Z | x | Y | Z | X | Y | z |
| $I_{(1)}$ | Static[a] | .694 | .242 | .340 | .1271 | .1140 | .2232 | .17845 | .33596 | .22279 |
| | vdW[b] | .672 | .240 | .322 | .1257 | .1260 | .2118 | .21015 | .34945 | .21904 |
| | Exp.[c] | .684 | .245 | .327 | .1260 | .1143 | .2136 | .20299 | .34045 | .22480 |
| $I_{(2)}$ | Static | .139 | .377 | .325 | .3732 | .6683 | .1655 | .99763 | .82672 | .32636 |
| | vdW | .137 | .360 | .327 | .3738 | .6571 | .1505 | .99716 | .82977 | .32768 |
| | Exp. | .145 | .372 | .328 | .3730 | .6825 | .1597 | .99639 | .82980 | .32908 |
| $O_{(1)}$ | Static | .302 | .045 | .738 | .0082 | .8529 | .1585 | .8424 | .2946 | .1546 |
| | vdW | .314 | .057 | .751 | .0108 | .8377 | .1487 | .8315 | .3036 | .1368 |
| | Exp. | .297 | .046 | .739 | .015 | .850 | .254 | .8448 | .3033 | .1461 |
| $O_{(2)}$ | Static | .306 | .039 | .092 | .1967 | .0381 | .4399 | .7949 | .6310 | .4767 |
| | vdW | .313 | .054 | .104 | .1956 | .0304 | .4416 | .7867 | .6249 | .4750 |
| | Exp. | .283 | .053 | .082 | .193 | .041 | .434 | .7856 | .6360 | .4835 |
| $O_{(3)}$ | Static | .690 | .153 | .549 | .4920 | .8435 | .3374 | .2488 | .2952 | .8957 |
| | vdW | .673 | .147 | .538 | .4974 | .8306 | .3453 | .2827 | .2991 | .9042 |
| | Exp. | .667 | .145 | .527 | .486 | .862 | .333 | .2617 | .2887 | .8894 |
| $O_{(4)}$ | Static | .952 | .245 | .964 | .3045 | .4864 | .2996 | .2439 | .6820 | .2900 |
| | vdW | .944 | .247 | .959 | .3050 | .4825 | .2992 | .2717 | .6858 | .2985 |
| | Exp. | .913 | .224 | .993 | .309 | .492 | .300 | .2506 | .6878 | .2990 |
| $O_{(5)}$ | Static | | | | .2503 | .9609 | .1225 | .1982 | .0408 | .1967 |
| | vdW | | | | .2527 | .9744 | .1152 | .2138 | .0441 | .1963 |
| | Exp. | | | | .250 | .968 | .116 | .2017 | .0462 | .1995 |
| $O_{(6)}$ | Static | | | | | | | .7888 | .0177 | .4168 |
| | vdW | | | | | | | .7593 | .0167 | .4085 |
| | Exp. | | | | | | | .7791 | .0180 | .4165 |

[a]Static calculation without the van der Waals correction.
[b]Static calculations with the van der Waals correction. The value of global scaling factor $s_6$ is the same as in Table I.
[c]Experimental data from Ref. 12 for $I_2O_4$, Ref. 18 for $I_2O_5$, and Ref. 13 for $I_2O_6$.

TABLE III. Important interatomic distances in crystalline $I_2O_4$. The subscript of the atom distinguishes symmetrically nonequivalent atoms, see Table II.

| Interatomic distances (Å) | | | | | |
|---|---|---|---|---|---|
| | | 0 GPa | | | 2 GPa |
| | | No vdW | With vdW | Exp.(300K) | With vdW |
| Intra-molecular | $I_{(1)}$-$O_{(3)}$ | 1.840 | 1.852 | 1.776(7) | 1.859 |
| | $I_{(1)}$-$O_{(4)}$ | 1.875 | 1.901 | 1.846(7) | 1.914 |
| | $I_{(2)}$-$O_{(1)}$ | 1.973 | 1.978 | 1.924(9) | 1.988 |
| | $I_{(2)}$-$O_{(2)}$ | 1.964 | 1.967 | 1.934(5) | 1.970 |
| Inter-molecular | $I_{(1)}$-$O_{(1)}$ | 2.132 | 2.120 | 2.054(6) | 2.094 |
| | $I_{(1)}$-$O_{(2)}$ | 2.170 | 2.20 | 2.150(5) | 2.201 |
| | $I_{(1)}$-$O_{(3)}$ | 2.491 | 2.437 | 2.607(7) | 2.387 |
| | $I_{(1)}$-$O_{(2)}$ | 2.997 | 2.797 | 2.884(6) | 2.673 |
| | $I_{(2)}$-$O_{(4)}$ | 2.548 | 2.490 | 2.598(6) | 2.417 |
| | $I_{(2)}$-$O_{(4)}$ | 2.673 | 2.598 | 2.691(6) | 2.552 |
| | $I_{(1)}$-$O_{(1)}$ | 3.364 | 3.047 | 3.136(7) | 2.951 |
| | $I_{(1)}$-$I_{(2)}$ | 3.553 | 3.578 | 3.465(7) | 3.566 |
| | $I_{(2)}$-$O_{(4)}$ | 3.368 | 3.351 | 3.226(6) | 3.399 |
| | $O_{(1)}$-$O_{(3)}$ | 2.775 | 2.753 | 2.675(5) | 2.699 |

slightly (from 0.75 to 1.0). For $I_2O_6$, we need a large modification of the $s_6$ (to 2.0) to reproduce the experimental volume at room temperature.

The calculations overestimate bond lengths in $I_2O_4$, $I_2O_5$, and $I_2O_6$ molecules in the three crystals (see Tables III–V). In most cases, overestimations are about 2–3% but in some cases they are as large as 5%. Although the vdW correction decreases the overall crystalline volume as shown in Table I, its effect on the bond lengths is nontrivial. The vdW correction in fact increases the bond lengths slightly in $I_2O_4$ with the largest increase about 1.3% in bond $I_{(1)}$-$O_{(4)}$ (The subscript distinguishes the nonequivalent atom in the primitive cell, see Table II). For $I_2O_5$, the lengths of all bonds except for $I_{(1)}$-$O_{(5)}$ increase by vdW correction. The change in bond length caused by vdW correction is mostly less than 1% except for $I_{(1)}$-$O_{(5)}$ and $I_{(2)}$-$O_{(3)}$, for which the bond length is decreased and increased, respectively, about 2%. For $I_2O_6$, the effect of vdW correction on the bond length depends on the iodine atom involved in the bond. The bond lengths involving $I_{(1)}$ atom increase, while those involving $I_{(2)}$ decrease, due to the vdW correction. The change of the bond lengths is usually small in $I_2O_6$.

TABLE IV. Important interatomic distances in crystalline $I_2O_5$. The subscript of the atom distinguishes symmetrically nonequivalent atom, see Table II.

| Interatomic distances (Å) | | | | | |
|---|---|---|---|---|---|
| | | 0 GPa | | | 2 GPa |
| | | No vdW | With vdW | Exp. (300K) | With vdW |
| Intra-molecular | $I_{(1)}$-$O_{(1)}$ | 1.875 | 1.889 | 1.78(3) | 1.921 |
| | $I_{(1)}$-$O_{(2)}$ | 1.828 | 1.847 | 1.77(3) | 1.879 |
| | $I_{(1)}$-$O_{(5)}$ | 1.987 | 1.947 | 1.92(2) | 1.945 |
| | $I_{(2)}$-$O_{(3)}$ | 1.902 | 1.946 | 1.83(3) | 1.981 |
| | $I_{(2)}$-$O_{(4)}$ | 1.821 | 1.830 | 1.79(3) | 1.851 |
| | $I_{(2)}$-$O_{(5)}$ | 2.020 | 2.042 | 1.95(3) | 2.056 |
| Inter-molecular | $I_{(1)}$-$O_{(1)}$ | 2.397 | 2.383 | 2.45(3) | 2.374 |
| | $I_{(1)}$-$O_{(1)}$ | 3.167 | 2.852 | 2.94(3) | 2.749 |
| | $I_{(1)}$-$O_{(2)}$ | 3.298 | 3.067 | 3.12(3) | 2.978 |
| | $I_{(1)}$-$O_{(4)}$ | 2.727 | 2.597 | 2.72(3) | 2.546 |
| | $I_{(2)}$-$O_{(2)}$ | 2.555 | 2.356 | 2.54(3) | 2.307 |
| | $I_{(2)}$-$O_{(3)}$ | 2.279 | 2.162 | 2.23(3) | 2.138 |
| | $I_{(2)}$-$O_{(3)}$ | 3.424 | 3.160 | 3.26(2) | 3.068 |
| | $I_{(2)}$-$O_{(4)}$ | 3.497 | 3.267 | 3.25(3) | 3.196 |

TABLE V. Important interatomic distance in crystalline $I_2O_6$. The subscript of the atom distinguishes symmetrically nonequivalent atom, see Table II.

| Interatomic distances (Å) | | | | | |
|---|---|---|---|---|---|
| | | 0 GPa | | | 2 GPa |
| | | No vdW | With vdW | Exp. (300K) | With vdW |
| Intra-molecular | $I_{(1)}$-$O_{(1)}$ | 1.770 | 1.785 | 1.754(9) | 1.785 |
| | $I_{(1)}$-$O_{(2)}$ | 2.027 | 2.062 | 1.962(7) | 2.064 |
| | $I_{(1)}$-$O_{(5)}$ | 2.051 | 2.079 | 1.967(8) | 2.075 |
| | $I_{(2)}$-$O_{(2)}$ | 1.998 | 1.980 | 1.946(8) | 1.972 |
| | $I_{(2)}$-$O_{(3)}$ | 1.876 | 1.881 | 1.798(8) | 1.879 |
| | $I_{(2)}$-$O_{(4)}$ | 1.883 | 1.876 | 1.798(9) | 1.871 |
| | $I_{(2)}$-$O_{(5)}$ | 1.986 | 1.964 | 1.922(7) | 1.954 |
| | $I_{(2)}$-$O_{(6)}$ | 2.011 | 2.000 | 1.951(8) | 1.995 |
| | $I_{(2)}$-$O_{(6)}$ | 2.023 | 2.016 | 1.957(8) | 2.010 |
| Inter-molecular | $I_{(1)}$-$O_{(3)}$ | 2.297 | 2.219 | 2.324(8) | 2.196 |
| | $I_{(1)}$-$O_{(4)}$ | 2.290 | 2.227 | 2.274(8) | 2.208 |

Regarding inter-molecular distances, the calculations without vdW correction overestimate most of them but also underestimate some of them. The vdW correction always decreases inter-molecular distances. In general, however, the vdW correction improves the agreement of the calculated inter-molecular distances with the experimental values (see Tables III–V).

We have found that the effect of vdW correction on structure is similar to the pressure effect. To show this, interatomic distances under a pressure of 2 GPa for the three crystals are also listed in Tables III–V. When a bond length increases/decreases with the vdW correction, it further increases/decreases with the pressure. As with vdW correction, (1) all bond lengths in $I_2O_4$ crystal increase slightly, (2) all bond lengths in $I_2O_5$ except for $I_{(1)}$-$O_{(5)}$ increase, and (3) the bond lengths involving $I_{(1)}$ atom increase and those involving $I_{(2)}$ decrease with the pressure in $I_2O_6$, with the pressure. Furthermore, the effects of vdW correction and the pressure are similar even in detail. For example, the length of $I_{(1)}$-$O_{(4)}$ bond changes more than the other bond lengths in $I_2O_4$ due to both vdW correction and pressure.

## B. Vibrational properties

The $I_2O_4$ and $I_2O_5$ crystals, with space group $P2_{1/c}$, have four molecules per unit cell. Therefore, there are 48 internal and 21 lattice modes for $I_2O_4$ crystal, whereas there are 60 internal and 21 lattice modes for $I_2O_5$ crystal. In a pure lattice mode, single molecule moves as a whole like a point; the vibration mainly results from the relative movement of molecules. Without inter-molecular interaction, the

internal modes should be four-folds degenerate. As listed in Tables III and IV, however, both crystals have some inter-molecular distances that are comparable to the bond lengths, implying strong inter-molecular interaction. The strong molecular interaction causes the mixture of internal modes and lattice modes. For $I_2O_6$ crystal, the basic molecular unit is actually $I_4O_{12}$ (see Fig. 3), and each unit cell has one $I_4O_{12}$ molecule. There are three lattice modes, all of which are libration modes, and 42 internal modes.

The calculated vibrational frequencies of the $I_2O_4$, $I_2O_5$, and $I_2O_6$ crystals with vdW correction are listed in Tables VI–VIII. The tables also list the "modes Grüneisen parameter," which is defined as $\gamma_i = -d\,\mathrm{Ln}\omega_i / d\,\mathrm{Ln}V$ and describes the volume ($V$) dependence of the frequency $\omega_i$ of the $i$th vibrational mode. For $I_2O_4$ crystal, the vibrational modes are divided into three groups: stretching modes with the highest frequencies, lattice modes with the lowest frequencies, and bending modes in the middle. The frequencies of the stretching modes are known to be sensitive to the bond length. As shown in Tables III–V, the calculation overestimates the bond length, which leads to overall underestimation of the stretching frequencies. In contrast, the calculated frequencies agree well with the experiment values in general for bending and lattice modes. In $I_2O_4$, the stretching and bending modes are clearly separated. The lowest frequency of the stretching modes is larger than the highest frequency of the bending modes by 80 $cm^{-1}$. Accordingly, the phonon density of states (PDOS) of $I_2O_4$ in Fig. 4 shows a clear gap between 425 and 488 $cm^{-1}$. Above the gap are the stretching modes. Since our calculation underestimates the frequencies of the stretching modes, we expect the real gap of $I_2O_4$ to be larger, and there should be no stretching modes with the frequency below 488 $cm^{-1}$. Consequently, the modes with the frequencies between 365–422 $cm^{-1}$, interpreted as stretching modes in the paper by Ellestad *et al.*[18] should be bending modes.

Modes Grüneisen parameters are usually positive. But for stretching modes in $I_2O_4$, modes Grüneisen parameters take small negative values. Namely, the frequencies of stretching modes decrease slightly with pressure. This is because the bond lengths of $I_2O_4$ increase with pressure as shown in Table III. Modes Grüneisen parameters are positive for

TABLE VI. Raman and infrared spectra for crystalline $I_2O_4$.

| Raman | | | | Infrared | | | | |
|---|---|---|---|---|---|---|---|---|
| This study | | | Exp.[a] | This study | | | Exp.[a] | |
| Freq. | Sym. | $\gamma$[c] | Freq. | Freq. | Sym. | $\gamma$ | Freq. | Assignment[b] |
| 749.4 | $B_g$ | −0.11 | 830 | 749.1 | $A_u$ | −0.17 | 825 | I2-O4 st |
| 654.2 | $A_g$ | −0.08 | 775 | 643.4 | $B_u$ | −0.21 | 779 | O4-I2-O3 sym. st+O2-I1-O1 sym. st |
| 627.3 | $A_g$ | −0.17 | 741 | 628.2 | $B_u$ | −0.52 | 750 | I2-O4 st+O2-I1-O1 sym. st |
| 600.5 | $B_g$ | −0.45 | 714 | 610.3 | $A_u$ | −0.40 | | I2-O3 st + I1-O2 st |
| 562.1 | $A_g$ | −0.23 | 637 | 563.6 | $B_u$ | −0.35 | 668 | O1-I1-O2 sym. st + O4-I2-O3 asym.st |
| 559.6 | $B_g$ | −0.21 | 617 | | | | | O2-I1-O1 sym. st |
| | | | | 559.6 | $A_u$ | −0.31 | 662 | I1-O1 st |
| 532.1 | $B_g$ | −0.29 | 540 | | | | | O1-I1-O2 asym st + I2-O3 st |
| | | | | 542.3 | $A_u$ | −0.26 | 623 | I2-O3 st +I1-O2 st |
| 489.8 | $A_g$ | −0.14 | 490 | 513.0 | $B_u$ | 0.0 | 576 | O1-I1-O2 asym st |
| 388.9 | $B_g$ | 0.77 | 401 | | | | | I1-O2 wagging + $IO_3$ bend |
| | | | | 392.7 | $B_u$ | 0.52 | 413 | O1-I1-O2 rock (out of the plane)+$IO_3$ bend |
| 372.9 | $B_g$ | 0.74 | 361 | | | | | O1-I1-O2 bend+ $IO_3$ bend |
| 369.6 | $A_g$ | 0.82 | 350 ? | | | | | I1-O2 wagging+ $IO_3$ bend |
| | | | | 376.7 | $A_u$ | 0.74 | 375 | I1-O2 wagging+ $IO_3$ bend |
| | | | | 353.3 | $A_u$ | 0.81 | | I1-O2 wagging+ $IO_3$ bend |
| 350.9 | $B_g$ | 0.61 | 332? | | | | | $IO_3$ bend+O2-I1-O1 rock (out of the plane) |
| | | | | 343.0 | $B_u$ | 0.63 | | O2-I1-O1 rock (in plane)+ $IO_3$ bend |
| 334.4 | $A_g$ | 0.71 | | | | | | $IO_3$ bend+O2-I1-O1 bend |
| | | | | 330.3 | $B_u$ | 0.65 | | O2-I1-O1 rock(in plane)+ $IO_3$ bend |
| 314.4 | $A_g$ | 0.39 | | | | | | $IO_3$ bend+O2-I1-O1 bend |
| | | | | 325.8 | $A_u$ | 0.66 | 326 | $IO_3$ bend+O2-I1-O1 rock |
| 313.0 | $A_g$ | 0.31 | | | | | | O2-I1-O1 bend+ $IO_3$ bend |
| 302.2 | $B_g$ | 0.28 | 305 | | | | | O2-I1-O1 + $IO_3$ bend |
| 286.4 | $B_g$ | 0.55 | | 285.5 | $B_u$ | 0.36 | | O2-I1-O1 bend+$IO_3$ bend |
| | | | | 277.5 | $A_u$ | 0.52 | 275 | O2-I1-O1 bend+$IO_3$ bend |
| 264.7 | $A_g$ | 0.36 | 262 | | | | | $IO_3$ rock+O2-I1-O1 rock |
| | | | | 251.9 | $B_u$ | 0.28 | 250 | $IO_3$ bend+O2-I1-O1 rock |
| 254.0 | $B_g$ | 0.99 | | | | | | $IO_3$ bend +O2-I1-O1 rock |
| | | | | 230.4 | $A_u$ | 0.59 | | $IO_3$ rock+O2-I1-O1 bend |
| 226.4 | $B_g$ | 1.25 | | | | | | O2-I1-O1 rock (in plane)+$IO_3$ rock |
| | | | | 225.6 | $B_u$ | 0.63 | 226 | $IO_3$ bend+O2-I1-O1 bend |

TABLE VI. (*Continued*).

| Raman | | | | Infrared | | | | |
|---|---|---|---|---|---|---|---|---|
| This study | | | Exp.[a] | This study | | | Exp.[a] | |
| Freq. | Sym. | $\gamma$[c] | Freq. | Freq. | Sym. | $\gamma$ | Freq. | Assignment[b] |
| 220.9 | $A_g$ | 0.62 | 230 | | | | | $IO_3$ bend+O2-I1-O1 bend |
| | | | | 220.3 | $A_u$ | 0.09 | 210 | O2-I1-O1 rock(in plane)+ $IO_3$ bend |
| 194.8 | $A_g$ | 1.23 | 191 | | | | | $IO_3$ rock |
| | | | | 194.8 | $B_u$ | 1.48 | 203 | O2-I1-O1 bend+$IO_3$ rock |
| 168.1 | $B_g$ | 0.48 | 180 | | | | | $IO_3$ rock O2-I1-O1 bend |
| | | | | 178.6 | $B_u$ | 0.83 | | O2-I1-O1 rock (in plane)+ $IO_3$ bend |
| 151.0 | $B_g$ | 0.87 | 161 | | | | | $IO_3$ rock+O2-I1 wagging |
| | | | | 178.5 | $A_u$ | 1.04 | | $IO_3$ rock |
| 144.7 | $A_g$ | 1.16 | 154 | | | | | O2-I1-O1 rock (in plane)+$IO_3$ bend |
| | | | | 157.5 | $B_u$ | 1.30 | 167 | O2-I1-O1 bend+ $IO_3$ bend |
| 131.8 | $B_g$ | 0.65 | 138 | | | | | |
| | | | | 141.9 | $A_u$ | 0.88 | 144 | $IO_3$ bend |
| 131.3 | $A_g$ | 0.80 | 128 | | | | | O2-I1-O1 rock (in plane) +lattice |
| | | | | 133.6 | $B_u$ | 1.35 | 134 | O2-I1-O1 rock (in plane)+lattice |
| 126.1 | $A_g$ | 0.78 | 128 | | | | | O2-I1-O1 rock (in plane)+ $IO_3$ rock |
| | | | | 124.5 | $A_u$ | 0.65 | | Lattice mode libration |
| 103.9 | $B_g$ | 1.68 | | | | | | Lattice mode translation |
| | | | | 110.1 | $A_u$ | 2.24 | 107 | $IO_3$ rock + lattice |
| 104.0 | $A_g$ | 1.24 | 100 | | | | | O1-I1 wagging +lattice |
| | | | | 102.3 | $B_u$ | 1.29 | 83 | O2-I1-O1 rock (out of the plane) + lattice |
| 86.6 | $B_g$ | 0.91 | | 83.1 | $A_u$ | 0.99 | 78 | Lattice mode libration |
| 85.2 | $A_g$ | 1.12 | 82 | 76.1 | $B_u$ | 1.70 | 69 | Lattice mode libration |
| 74.4 | $B_g$ | 1.27 | 74 | | | | | Lattice mode translation |
| | | | | 55.1 | $A_u$ | 0.6 | 62 | Lattice mode libration |
| 69.9 | $B_g$ | 2.07 | | | | | | Lattice mode translation |
| 68.5 | $A_g$ | 1.07 | 58 | | | | | Lattice mode libration |
| 42.8 | $A_g$ | 1.62 | | | | | | Lattice mode translation |

[a]Reference 18.
[b]The modes are assigned according to the movement of one molecule, whereas the movement of the other molecules in the unit cell are found from symmetry. The atom index in the molecule is defined in Fig. 1(b). St stands for stretch, sym. st for symmetric stretch, and asym. st for antisymmetric stretch.
[c]Modes Grüneisen parameter, defined as $\gamma_i = -d\,\mathrm{Ln}\omega_i / d\,\mathrm{Ln}V$, describes the volume dependence of the $i$th frequency mode.

all other modes, and are usually smaller than unity for the bending modes and larger than unity for the lattice modes.

Similar to the case of $I_2O_4$, the stretching and bending modes are separated in $I_2O_5$ crystal. However, the gap between them, which is located between 425 and 439 $cm^{-1}$ (see Fig. 5), is far smaller than that in $I_2O_4$. The calculation also underestimates the frequencies of the stretching modes in $I_2O_5$. For the lattice and bending modes, the calculation generally agrees with experiment. In Table VII, the symmetric and asymmetric stretching modes are also separated. The symmetric stretching modes have frequencies larger than 690 $cm^{-1}$, while the asymmetric stretching modes have frequencies smaller than 640 $cm^{-1}$. At 700 $cm^{-1}$, the phonon density of states of $I_2O_5$ is considerably small (see Fig. 5). Our calculation shows that the phonon density of states above this frequency comes from symmetric stretching modes and that between 439 and 700 $cm^{-1}$ comes from asymmetric stretching modes. The modes Grüneisen parameters of the stretching modes are small and most (but not all) of them are negative. In contrast to $I_2O_4$, where all bond lengths increase with pressure, some bond lengths decrease with pressure in $I_2O_5$. This explains why modes Grüneisen parameters of some stretching modes are still positive. As in the case of $I_2O_4$ crystal, the lattice modes of $I_2O_5$ have significantly larger modes Grüneisen parameters than other modes, which reflects the fact that inter-molecular distances are greatly reduced by pressure (see Tables III–V).

For crystalline $I_2O_6$, no experimental Raman or infrared spectra are available to the best of our knowledge. However, since the calculation overestimates the bond lengths, we believe that the frequencies of stretching modes should be underestimated in our calculation. Our calculations predict that crystalline $I_2O_6$ has vastly different vibrational properties compared to $I_2O_4$ and $I_2O_5$ crystals. For example, the stretching modes are not separated from other kinds of modes. Furthermore, two of the stretching modes have frequencies far larger than the other modes, creating a large gap in the phonon density of states (see Fig. 6). Also, the two highest-frequency stretching modes are the only two modes with small negative modes Grüneisen parameters. As in the case of $I_2O_4$ and $I_2O_5$, the modes Grüneisen parameters of the

TABLE VII. Raman and infrared spectra for crystalline $I_2O_5$.

| Raman | | | | Infrared | | | | |
|---|---|---|---|---|---|---|---|---|
| This study | | | Exp.[a] | This study | | | Exp.[a] | |
| Freq. | Sym. | $\gamma$[c] | Freq. | Freq. | Sym. | $\gamma$[a] | Freq. | Assignment[b] |
| 765.6 | $A_g$ | 0.04 | 834 | | | | | O3-I1-O2 st + O4-I2-O3 st |
| 757.9 | $B_g$ | − 0.11 | 831 | 757.5 | $A_u$ | − 0.05 | 835 | I2-O4 st |
| | | | | 757.1 | $B_u$ | − 0.15 | 820 | $IO_3$ st |
| 734.8 | $B_g$ | 0.20 | 810 | | | | | O1-I1-O2 st |
| | | | | 728.2 | $A_u$ | − 0.25 | 800 | I1-O2 st |
| 705.0 | $A_g$ | − 0.08 | 748 | | | | | I1-O2 st + I2-O4 st |
| | | | | 705.6 | $B_u$ | − 0.09 | 755 | O1-I1-O2 st + I2-O4 st |
| 641.7 | $B_g$ | − 0.24 | 724 | | | | | O3-I1-O1 st + IO3 (I2) asym. st |
| | | | | 694.5 | $B_u$ | − 0.22 | 720 | I1-O1 + I2-O5 st |
| 606.4 | $A_g$ | 0.06 | 693 | | | | | $IO_3$ (I1) asym.st + I2-O3 st |
| | | | | 592.2 | $B_u$ | 0.18 | 670 | O3-I2-O5 st + O2-I1-O3 asym. st |
| 583.7 | $B_g$ | − 0.04 | 607 | | | | | $IO_3$ asym.st + O3-I2-O5 st |
| | | | | 590.4 | $A_u$ | 0.13 | | O1-I1-O3 asym.st + I2-O3 st |
| 578.2 | $A_g$ | − 0.07 | | 568.9 | $A_u$ | − 0.12 | 587 | O3-I1-O1 st + O5-I2-O3 asym st |
| 468.9 | $A_g$ | 0.44 | 535 | 483.8 | $A_u$ | 0.02 | 510 | I2-O5 st |
| 436.6 | $B_g$ | 0.57 | 433 | | | | | O3-I2-O5 asym. St + O3-I1st |
| | | | | 429.5 | $B_u$ | 0.61 | | O3-I2-O5 asym. St + O3-I1-O1 asym. st |
| 414.4 | $B_g$ | 0.44 | 412 | 398.7 | $B_u$ | 0. 35 | 415 | O5-I2-O4 bend |
| 388.8 | $A_g$ | 0.32 | 401 | 392.5 | $A_u$ | 0.37 | | $IO_3$ bend |
| 383.0 | $B_g$ | 0.38 | 377 | 379.3 | $B_u$ | 0.29 | | $IO_3$ bend |
| 361.6 | $B_g$ | 0.38 | 361 | 350.0 | $A_u$ | 0.57 | 357 | $IO_3$ bend |
| 353.3 | $A_g$ | 0.58 | | 329.9 | $B_u$ | 0.85 | 340 | $IO_3$ bend |
| 337.8 | $A_g$ | 0.69 | | 314.9 | $A_u$ | 0.66 | 327 | $IO_3$ bend |
| 314.2 | $A_g$ | 0. 24 | 323 | 304.0 | $B_u$ | 0.37 | 305 | $IO_3$ bend |
| 312.1 | $B_g$ | 0.59 | | 298.6 | $A_u$ | 0.55 | | $IO_3$ bend |
| 286.2 | $B_g$ | 0.78 | 300 | 287.9 | $B_u$ | 0.76 | | $IO_3$ bend |
| 280.7 | $A_g$ | 0.44 | | 280.7 | $A_u$ | 0.44 | 276 | $IO_3$ bend |
| 265.0 | $B_g$ | 0.40 | | 259.4 | $B_u$ | 0.63 | | $IO_3$ bend |
| 256.7 | $A_g$ | 0.67 | 263 | 255.2 | $A_u$ | 0.63 | | $IO_3$ bend |
| 250.3 | $B_g$ | 0.68 | | 252.8 | $B_u$ | 0.62 | | $IO_3$ bend (I1) +$IO_3$ rock (I2) |
| 213.7 | $B_g$ | 0.68 | | 217.5 | $A_u$ | 0.06 | 222 | $IO_3$ bend (I1) + $IO_3$ rock (I2) |
| 213.8 | $A_g$ | 0.50 | | 214.6 | $B_u$ | 0.61 | | $IO_3$ bend |
| 199.0 | $A_g$ | 0.73 | 202 | 200.0 | $A_u$ | 0.53 | 205 | $IO_3$ bend |
| 191.4 | $B_g$ | 0.59 | 193 | | | | | $IO_3$ rock |
| 181.2 | $A_g$ | 0.61 | | 174.5 | $A_u$ | 0.73 | 180 | $IO_3$ bend (I2) + $IO_3$ rock (I1) |
| 171.0 | $B_g$ | 0.82 | 176 | 169.4 | $B_u$ | 0.89 | | $IO_3$ rock |
| 156.9 | $A_g$ | 0.65 | | 148.7 | $B_u$ | 1.42 | | $IO_3$ rock |
| | | | | 149.0 | $A_u$ | 1.02 | 153 | $IO_3$ rock (I1)+$IO_3$ bend (I2) |
| 150.3 | $B_g$ | 0.44 | 146 | | | | | Lattice libration |
| 140.0 | $A_g$ | 0.83 | | | | | | $IO_3$ rock (I1)+$IO_3$ bend (I2) |
| | | | | 132.8 | $B_u$ | 1.20 | | $IO_3$ rock (I2)+$IO_3$ bend (I1) |
| 122.5 | $A_g$ | 1.22 | | 128.0 | $A_u$ | 1.31 | | $IO_3$ rock |
| | | | | 122.3 | $A_u$ | 0.68 | 122 | Lattice libration |
| 110.6 | $B_g$ | 0.81 | 109 | 112.7 | $B_u$ | 0.91 | | Lattice libration |
| 105.4 | $A_g$ | 0.69 | | | | | | Lattice translation |
| 103.4 | $B_g$ | 0.34 | 97 | 107.6 | $A_u$ | 1.04 | 109 | Lattice translation |
| | | | | 90.2 | $A_u$ | 1.17 | | Lattice libration |
| 81.3 | $B_g$ | 1.21 | | 89.5 | $B_u$ | 1.07 | 87 | Lattice libration |
| 81.1 | $A_g$ | 1.34 | 80 | 76.2 | $B_u$ | 1.35 | 81 | Lattice libration |
| 62.3 | $B_g$ | 1.60 | 65 | | | | | Lattice translation |
| | | | | 62.2 | $A_u$ | 1.34 | | Lattice libration |
| 58.9 | $A_g$ | 1.41 | 59 | | | | | Lattice translation |
| 49.0 | $A_g$ | 1.26 | | | | | | Lattice translation |
| 41.1 | $B_g$ | 1.28 | 47 | | | | | Lattice libration |

[a]Reference 18.

[b]The modes are assigned according to the movement of one molecule, whereas the movement of the other molecules in the unit cell are found from symmetry. The atom index in the molecule is defined in Fig. 1(b). St stands for stretch, sym. st for symmetry stretch, and asym. st for antisymmetry stretch.

[c]Modes Grüneisen parameter, defined as $\gamma_i = -d\ \mathrm{In}\omega_i / d\ \mathrm{In}V$, describes the volume dependence of the $i$th frequency mode.

TABLE VIII. Raman and infrared spectra for $I_2O_6$ crystal.

| Raman | | | Infrared | | |
|---|---|---|---|---|---|
| This study | | Exp. | This study | | |
| Freq. | $\gamma$[b] | Freq. | Freq. | $\gamma$[b] | Assignment[a] |
| 845.5 | −0.11 | 893.2 | 846.4 | −0.11 | I-O st (I1-O2, I2-O11) |
| 670.4 | 0.78 | 779.8 | 653.5 | 0.89 | $IO_6$ st |
| 598.4 | 0.77 | 716.3 | 617.7 | 0.58 | $IO_6$ st |
| 593.2 | 0.74 | 654.5 | | | $IO_2$ sci (O8-I3-O5, O18-I4-O19) |
| | | | 561.0 | 0.81 | $IO_2$ rock (O8-I3-O5, O18-I4-O19) |
| 493.7 | 1.11 | 570.3 | | | $IO_2$ asy st (O6-I3-O3, O7-I4-O10) |
| | | | 515.7 | 0.64 | $IO_2$ asy st (O6-I3-O3, O7-I4-O10)+$IO_2$ bend (O8-I3-O5, O8-I4-O5) |
| 484.6 | 0.87 | 482.5 | | | $IO_2$ asy st (O9-I3-O12, O4-I4-O1) |
| | | | 499.8 | 0.89 | $IO_2$ asy st (O9-I3-O12, O4-I4-O1)+$IO_2$ bend (O8-I3-O5, O8-I4-O5) |
| 471.6 | 0.67 | | | | $IO_2$ rock (O8-I3-O5, O18-I4-O19) |
| | | | 458.2 | 0.95 | $IO_2$ asy st (O3-I3-O12, O10-I4-O1)+$IO_2$ bend (O8-I3-O5, O8-I4-O5) |
| 433.9 | 0.65 | | | | $IO_2$ rock (O1-I1-O3, O10-I2-O12)+$IO_2$ rock (O8-I3-O5, O8-I4-O5) |
| | | | 444.0 | 0.42 | $IO_2$ sci (O1-I1-O3, O10-I2-O12)+$IO_2$ bend (O8-I3-O5, O8-I4-O5) |
| 433.0 | 0.26 | 404.9 | | | $IO_2$ sci (O1-I1-O3, O10-I2-O12), |
| | | | 401.1 | 0.5 | $IO_2$ rock (O1-I1-O3, O10-I2-O12), |
| 370.0 | 0.68 | 375.8 | | | $IO_3$ rock (I1,I2)+$IO_2$ sci (O7-I4-O4,O9-I3-O6) |
| | | | 366.8 | 0.71 | Ring bend (I3-O8-I4-O5){folding} |
| 342.2 | 0.85 | 359.6 | | | Ring rock (I3-O8-I4-O5)+$IO_3$ bend (I1,I2), |
| | | | 352.3 | 0.41 | $IO_3$ rock (I1,I2)+$IO_2$ sci (O7-I4-O4,O9-I3-O6) |
| 336.1 | 0.54 | 312.9 | | | $IO_3$ rock (I1,I2), |
| | | | 313.3 | 0.74 | Ring (I3-O8-I4-O5) bend {folding}+$IO_3$ bend (I1,I2) |
| 285.4 | 1.09 | 279.9 | | | $IO_3$ st (I1,I2), $IO_2$ rock (O7-I4-O4,O9-I3-O6) {out of $I_2O_4$ plane} |
| | | | 285.0 | 0.83 | $IO_3$ bend (I1,I2) + $IO_2$ rock (O7-I4-O4,O9-I3-O6) {in $I_2O_4$ plane} |
| 278.0 | 0.79 | 262.4 | | | $IO_2$ rock (O7-I4-O4,O9-I3-O6) {in $IO_2$ plane} + $IO_2$ rock (I1-O3- O1, I2-O10-O12) |
| | | | 259.0 | 0.70 | $IO_2$ rock (O7-I4-O4,O9-I3-O6){out of $IO_2$ plane} + $IO_2$ rock(I1-O3-O1, I2-O10-O12) |
| 255.4 | 0.83 | 240.9 | | | Ring rock (I3-O8-I4-O5), $IO_3$ bend |
| | | | 230.6 | 0.03 | $IO_2$ rock (I1-O3-O1, I2-O10-O12)+$IO_2$ sci (O7-I4-O4,O9-I3-O6) |
| 213.4 | 0.71 | 222.9 | | | Wagging (I2-O11, I1-O2) |
| | | | 205.6 | 1.47 | $IO_3$ bend |
| 204.7 | 1.12 | 201.2 | | | $IO_3$ rock |
| | | | 195.4 | 0.31 | Wagging (I2-O11, I1-O2) |
| 195.1 | 0.44 | | | | Wagging (I2-O11, I1-O2) |
| | | | 189.3 | 0.51 | Ring bend (I3-O8-I4-O5) {folding}, $IO_2$ rock (O2-I1-O3, O11-I2-O10) |
| 190.9 | 0.98 | | | | $IO_3$ bend |
| | | | 167.2 | 0.63 | $IO_3$ rock |
| 179.9 | 0.46 | | | | $IO_2$ rock (O7-I4-O4,O9-I3-O6) {in $I_2O_4$ plane} |
| | | | 148.3 | 0.77 | $IO_3$ rock |
| 130.4 | 0.65 | 143.7 | | | $IO_2$ bend (I1-O3-O1, I2-O10-O12) |
| | | | 138.7 | 0.71 | $IO_3$ rock |
| 126.7 | 1.26 | 114.1 | | | Lattice modes |
| 99.5 | 0.97 | 101.6 | | | Lattice modes |
| 79.5 | 1.28 | 81.3 | | | Lattice modes |

[a]The atom index is shown in Fig. 3(b). St stands for stretch, asy st for antisymmetry stretch, and sci for scissor.
[b]Modes Grüneisen parameter, defined as $\gamma_i = -d\ \mathrm{In}\omega_i / d\ \mathrm{In}V$, describes the volume dependence of the $i$th frequency mode.

lattice modes are usually larger than those of most other modes.

We have also found that partial iodine and oxygen contributions to the phonon density of states are significantly different in $I_2O_4$, $I_2O_5$, and $I_2O_6$ as shown, respectively, in Figs. 4(b), 5(b), and 6(b). The partial iodine and oxygen phonon density of states exhibit almost the same pattern in $I_2O_4$ and $I_2O_5$ except that the partial phonon density of states of Iodine is much smaller than that of Oxygen, mainly because the number of I atoms are smaller than that of O atoms. These partial contributions indicate that the vibrational modes in $I_2O_5$ always involve noticeable movements of both I and O atoms. This is also true for $I_2O_4$ for the modes with frequencies less than 700 $cm^{-1}$. But for modes with frequencies above 700 $cm^{-1}$, I atoms have much smaller contribution to the phonon density of states. In $I_2O_6$, I atoms contribute to the phonon density of states only for low-frequency modes. For all modes with frequencies above 300 $cm^{-1}$, I atoms are not contributing to the vibrational modes.

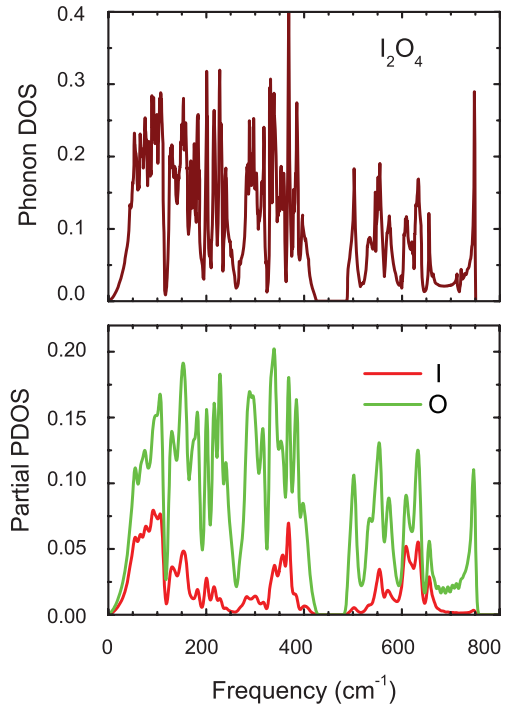


FIG. 4. (a) Phonon density of states and (b) partial phonon density of states of $I_2O_4$ crystal at 0 GPa with vdW correction.

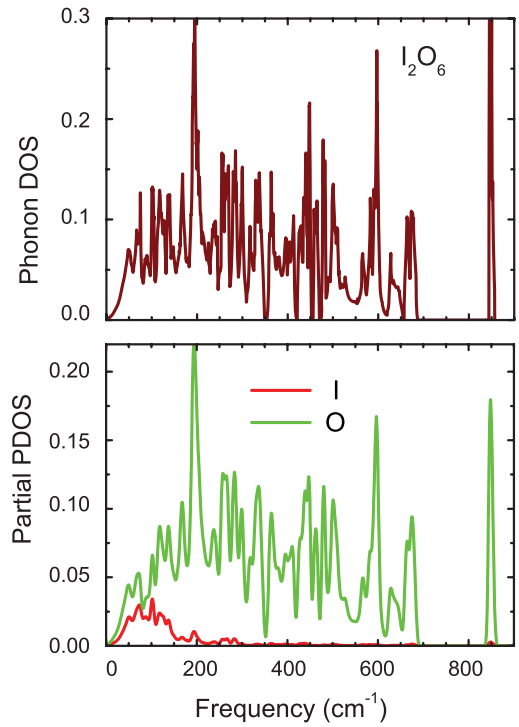


FIG. 6. (a) Phonon density of states and (b) partial phonon density of states of $I_2O_6$ at 0 GPa with vdW correction.

### C. Thermodynamic properties

The equation of state of the three crystals, $I_2O_4$, $I_2O_5$, and $I_2O_6$, are shown in Fig. 7. As has been discussed in Sec. III, the calculation without vdW correction overestimates the volume significantly. However, at high pressures, the vdW correction has less effect on volume for all three crystals. Volume difference at 0 GPa between calculations with and without vdW correction is 9.6%, 12.0%, and 13.2%, respectively, for $I_2O_4$, $I_2O_5$, and $I_2O_6$. At 5 GPa, the difference decreases to 3.1%, 4.5%, and 5.7%, respectively, for $I_2O_4$, $I_2O_5$, and $I_2O_6$.

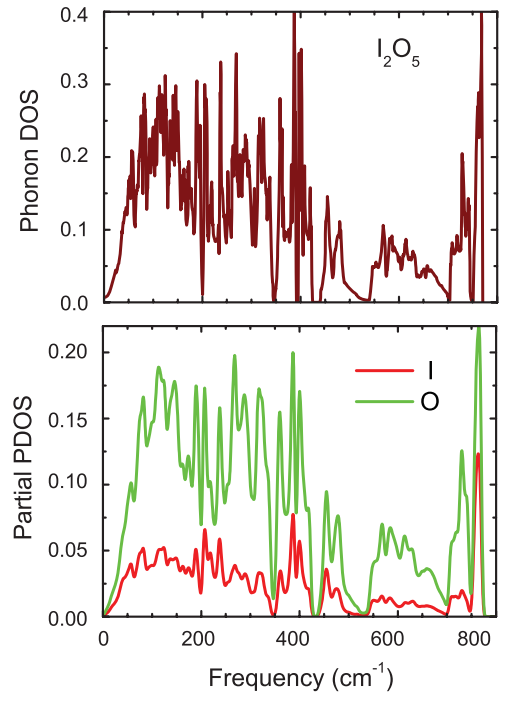


FIG. 5. (a) Phonon density of states and (b) partial phonon density of states of $I_2O_5$ crystal at 0 GPa with vdW correction.

Fig. 7 also shows that the vibrational contribution noticeably increases the equilibrium volume. The effect of zero-point motion and room temperature shifts the equilibrium volume by 1.3%, 2.2%, and 0.9%, respectively, for $I_2O_4$, $I_2O_5$, and $I_2O_6$. Interestingly, these values are very similar to those in materials such as MgO and $Mg_2SiO_4$,[29–32] although the bulk moduli of MgO and $Mg_2SiO_4$ (about 170 GPa) are far larger than those of iodine-oxide crystals (about 30 GPa). As mentioned in Sec. II, we modify the $s_6$ value in the vdW correction, Eq. (3), to reproduce the experimental equilibrium volume at room temperature. Therefore resulting EOS should be quite accurate at low pressures, and is expected to provide a reasonable prediction of the volume at high pressures and temperatures.

Thermodynamic properties of the three materials, including thermal expansion, heat capacity, adiabatic bulk modulus, and thermal Grüneisen parameter, are shown in Figs. 8–10. The thermodynamic data at ambient condition are listed in Table IX. Thermal expansion coefficient increases rapidly as a function of temperature up to about 250 K, and then increases slightly with temperature at higher temperatures. This is because the thermal expansion is proportional to the heat capacity at constant volume. The thermal expansion is reflecting the behavior of heat capacity as a function of

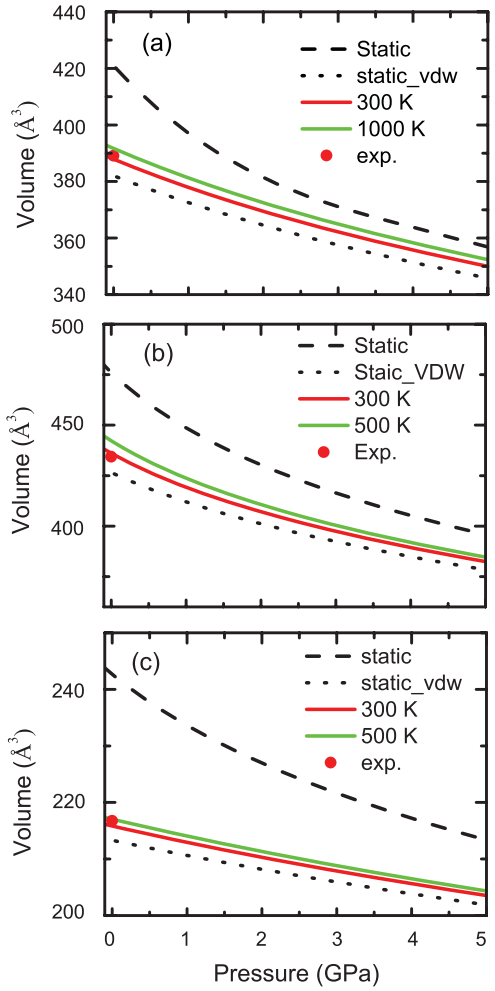


FIG. 7. Equation of state of (a) $I_2O_4$, (b) $I_2O_5$, and (c) $I_2O_6$. Experimental data are from Ref. 8 for $I_2O_4$, Ref. 10 for $I_2O_5$, and Ref. 9 for $I_2O_6$.

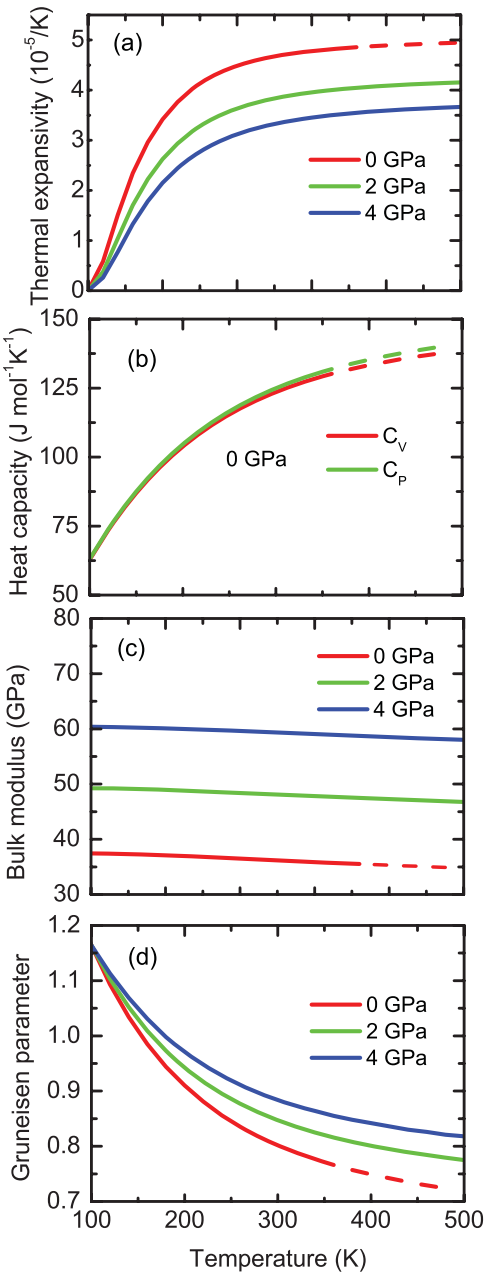


FIG. 8. Thermodynamic properties of $I_2O_4$ as a function of temperature. (a) thermal expansion, (b) heat capacity at constant volume $C_V$ and pressure $C_P$, (c) adiabatic bulk modulus, and (d) thermal Grüneisen parameter.

temperature, which shows saturation as a function of temperature. The bulk modulus decreases almost linearly with temperature. The bulk modulus of $I_2O_5$ is the smallest among the three crystals. $I_2O_6$ has much larger bulk modulus than $I_2O_4$ and $I_2O_5$. The densities of the three materials follow the sequence, $\rho_{I_2O_5} < \rho_{I_2O_4} < \rho_{I_2O_6}$, which is opposite to the bulk-modulus sequence. Namely, for normal crystals the denser is the crystal, the larger is the bulk modulus. In contrast, the thermal expansivity, $\alpha$, for the three materials follows the counter intuitive behavior as expected from the bulk modulus, i.e., $\alpha_{I_2O_5} > \alpha_{I_2O_4} > \alpha_{I_2O_6}$. This is because the three crystals have similar thermal pressure gradients about 0.0017 GPa/K, and the thermal pressure gradient is the product of the bulk modulus and thermal expansivity, $\alpha K_T = (\partial P/\partial T)_V$.

The thermal Grüneisen parameter, which is defined as $\gamma_{th} = \alpha K_T V/C_V$, is the weighted average of the modes Grüneisen parameters. At low temperatures, the thermal Grüneisen parameter is determined mostly by low-frequency modes. As shown in Tables III–V, low-frequency modes (which are lattice modes) have larger modes Grüneisen parameters than other modes. This is why the thermal Grüneisen parameter decreases with temperature as shown in Figs. 8–10. At increased temperatures, all the modes tend to contribute equally, and hence the thermal Grüneisen parameter becomes close to the average value of the modes Grüneisen parameters. Consequently, the thermal Grüneisen parameter becomes almost temperature independent at sufficiently high temperatures.

The heat capacities at constant pressure, $C_P$, and constant volume, $C_V$, are related by $C_P = (1 + \alpha\gamma_{th}T)C_V$. Heat capacity increases rapidly below about the 250 K and saturates at high temperatures. Since the quasi-harmonic approximation is used in the calculation, $C_V$ is subjected to the law of Dulong and Petit. However, $C_P$ can be significantly larger than the Dulong-Petit limit.

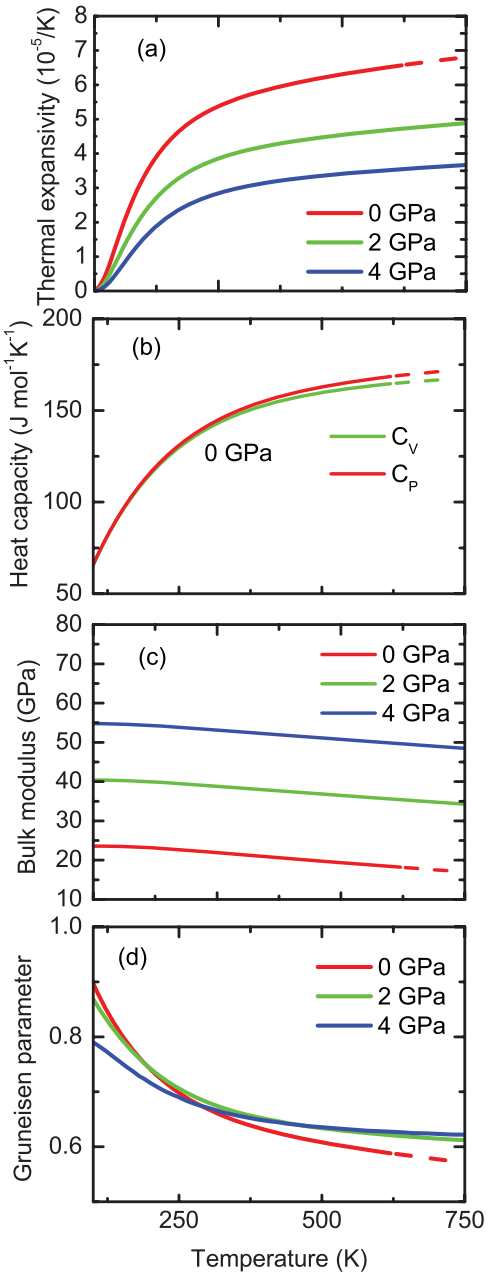


FIG. 9. Thermodynamic properties of $I_2O_5$ as a function of temperature. (a) Thermal expansion, (b) heat capacity at constant volume $C_V$ and pressure $C_P$, (c) adiabatic bulk modulus, and (d) thermal Grüneisen parameter.

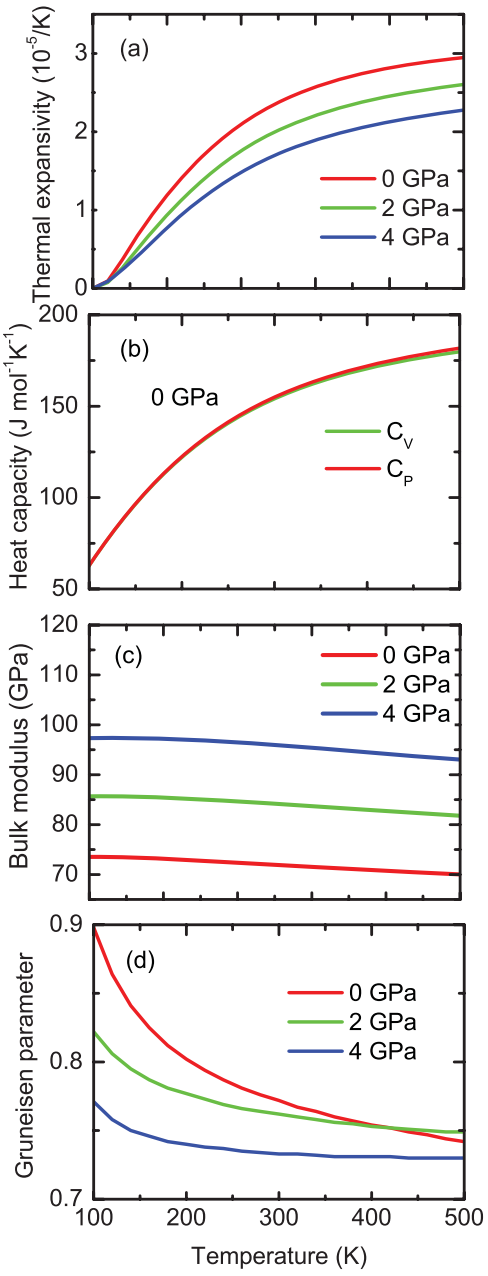


FIG. 10. Thermodynamic properties of $I_2O_6$ as a function of temperature. (a) Thermal expansion, (b) heat capacity at constant volume $C_V$ and pressure $C_P$, (c) adiabatic bulk modulus, and (d) thermal Grüneisen parameter.

TABLE IX. Thermodynamic data at ambient condition.

| | Volume (Å$^3$/cell) | Bulk modulus $K_T$ (GPa) | Pressure derivative of bulk modulus $K_T$' | *Thermal expansion* $\alpha$ ($10^{-5}$/K) | *Heat capacity* $C_P$ (J/mol/K) | Grüneisen parameter $\gamma$ |
|---|---|---|---|---|---|---|
| $I_2O_4$ | 387.86 | 35.4 | 6.19 | 4.78 | 124.9 | 0.8 |
| $I_2O_5$ | 436.05 | 21.3 | 9.78 | 5.65 | 141.7 | 0.7 |
| $I_2O_6$ | 215.83 | 71.1 | 6.22 | 2.57 | 154.9 | 0.8 |

## IV. CONCLUSION

The van de Waals correction in DFT within GGA is important in first principles investigation of molecular crystals such as iodine oxides. The volume calculated without vdW correction is larger than experimental equilibrium volume by 7.9%, 9.9%, and 11.7%, respectively, for $I_2O_4$, $I_2O_5$, and $I_2O_6$. With the vdW correction, the calculated volumes for the three systems agree well with the experimental volumes. The effect of the vdW correction on lattice constant has been found to be highly anisotropic reflecting the crystal structures. For example, $I_2O_4$ crystal can approximately be viewed as one-dimension solid, comprising infinite ●●●-I-O-$IO_2$-O-●●● chains along the *c* direction. Accordingly, the vdW correction on lattice constant in the *c* direction is much smaller compared with the other directions. We have also found the vdW effect on crystalline structure is very similar to the pressure effect. Both decrease the inter-molecular distances but can slightly increase some bond lengths. This unusual feature results in the decrease of frequencies of some stretching modes with pressure, i.e., some stretching modes have negative "modes Grüneisen parameters."

All three iodine oxide crystals have a gap in the phonon density of states but with different characteristics. The gap in $I_2O_4$ is much larger than that of $I_2O_5$, which separate the stretching modes from the other modes. Namely, all vibrational modes are stretching modes above the gap. In $I_2O_5$, the symmetric and asymmetric stretching modes are further separated at frequencies about 700 $cm^{-1}$, at which the phonon density of states is considerably small. For $I_2O_6$, the gap lies within the frequency range of the stretching modes. Above the gap are two highest frequency stretching modes with negative modes Grüneisen parameters. In contrast, all modes below the gap have positive modes Grüneisen parameters. In all three crystals, lattice modes have in general larger modes Grüneisen parameters than other modes, which reflect the fact that inter-molecular distances are greatly reduced by pressure.

The vibrational contribution noticeably increases the equilibrium volume at the room temperature. The effect of zero-point motion and room temperature increase the equilibrium volume by 1∼2%. This shift is similar to those of MgO and $Mg_2SiO_4$, although they have the bulk modulus far larger than the iodine oxide crystals. The $I_2O_4$, $I_2O_5$, and $I_2O_6$ have distinct thermodynamic properties. The bulk modulus of $I_2O_6$ is far larger than those of $I_2O_4$ and $I_2O_5$, whereas the thermal expansion of $I_2O_6$ is much smaller than those of $I_2O_4$ and $I_2O_5$. Nevertheless, the product of bulk modulus and thermal expansion, i.e., thermal pressure gradient, is nearly the same for the three materials.

## ACKNOWLEDGMENTS

This research was supported by the Defense Threat Reduction Agency, Grant No. HDTRA1-08-1-0036. Authors would like to thank Professors Karl Christe and Rolf Haiges for many critical discussions about synthesis and properties of the I2Ox compounds, and Dr. Suhithi Peiris for encouragement and continued support for this research project. Computations were performed at the University of Southern California using the 119.6 teraflops Linux cluster at the Research Computing Facility and the 2048-processor Linux cluster at the Collaboratory for Advanced Computing and Simulations.

[1] R. W. Saunders and J. M. C. Plane, Environ. Chem. **2**, 299 (2005).
[2] C. D. O'dowd, J. L. Jimenez, R. Bahreini, R. C. Flagan, J. H. Seinfeld, K. Hameri, L. Pirjola, M. Kulmala, S. G. Jennings, and T. Hoffmann, Nature (London) **417**, 632 (2002).
[3] A. Saiz-Lopez, J. M. C. Plane, G. McFiggans, P. I. Williams, S. M. Ball, M. Bitter, R. L. Jones, C. Hongwei, and T. Hoffmann, Atmos. Chem. Phys. **6**, 883 (2006).
[4] G. McFiggans, H. Coe, R. Burgess, J. Allan, M. Cubison, M. R. Alfarra, R. Saunders, A. Saiz-Lopez, J. M. C. Plane, D. J. Wevill, L. J. Carpenter, A. R. Rickard, and P. S. Monks, Atmos. Chem. Phys. **4**, 701 (2004).
[5] J. L. Jimenez, J. T. Jayne, Q. Shi, C. E. Kolb, D. R. Worsnop, I. Yourshaw, J. H. Seinfeld, R. C. Flagan, X. F. Zhang, K. A. Smith, J. W. Morris, and P. Davidovits, J. Geophys. Res., [Atmos.] **108**(D7), 8425 (2003).
[6] J. B. Burkholder, J. Curtius, A. R. Ravishankara, and E. R. Lovejoy, Atmos. Chem. Phys. **4**, 19 (2004).
[7] C. D. O'dowd and T. Hoffmann, Environ. Chem. **2**, 245 (2005).
[8] S. Schneider, R. Haiges, T. Schroer, J. Boatz, and K. O. Christe, Angew. Chem., Int. Ed. **43**, 5213 (2004).
[9] R. A. Yetter, F. L. Dryer, M. T. Allen, and J. L. Gatto, J. Propul. Power **11**, 683 (1995).
[10] K. L. McNesby, A. W. Miziolek, T. Nguyen, F. C. Delucia, R. R. Skaggs, and T. A. Litzinger, Combust. Flame **142**, 413 (2005).
[11] K. K. Kuo, *Principles of Combustion* (John Wiley & Sons, New York, 1986).
[12] H. Fjellvag and A. Kjekshus, Acta Chem. Scand. **48**, 815 (1994).
[13] T. Kraft and M. Jansen, J. Am. Chem. Soc. **117**, 6795 (1995).
[14] K. Selte and A. Kjekshus, Acta Chem. Scand. **24**, 1912 (1970).
[15] M. S. Lehmann, A. N. Christensen, H. Fjellvag, R. Feidenhansl, and M. Nielsen, J. Appl. Crystallogr. **20**, 123 (1987).
[16] W. E. Dasent and T. C. Waddington, J. Chem. Soc., 2429 (1960).
[17] W. E. Dasent and T. C. Waddington, J. Chem. Soc., 3350 (1960).
[18] O. H. Ellestad, T. Woldbaek, A. Kjekshus, P. Klaeboe, and K. Selte, Acta Chem. Scand., Ser. A **35**, 155 (1981).
[19] J. H. Wise and H. H. Hannan, J. Inorg. Nucl. Chem. **23**, 31 (1961).
[20] P. M. Sherwood and J. J. Turner, Spectrochim. Acta, Part A **A 26**, 1975 (1970).
[21] S. P. Karna, J. Phys. Chem. A **104**, 4671 (2000).
[22] M. Alcami, O. Mo, M. Yanez, and I. L. Cooper, J. Phys. Chem. A **103**, 2793 (1999).
[23] A. Misra and P. Marshall, J. Phys. Chem. A **102**, 9056 (1998).
[24] S. Roszak, M. Krauss, A. B. Alekseyev, H. P. Liebermann, and R. J. Buenker, J. Phys. Chem. A **104**, 2999 (2000).
[25] B. Minaev, O. Loboda, O. Vahtras, H. Agren, and E. Bilan, Spectrochim. Acta, Part A **58**, 1039 (2002).
[26] N. Kaltsoyannis and J. M. C. Plane, Phys. Chem. Chem. Phys. **10**, 1723 (2008).
[27] S. Baroni, S. de Gironcoli, A. Dal Corso, and P. Giannozzi, Rev. Mod. Phys. **73**, 515 (2001).
[28] Z. Q. Wu and R. M. Wentzcovitch, Phys. Rev. B **79**, 104304 (2009).
[29] B. B. Karki, R. M. Wentzcovitch, S. de Gironcoli, and S. Baroni, Phys. Rev. B **61**, 8793 (2000).
[30] L. Li, R. M. Wentzcovitch, D. J. Weidner, and C. R. S. Da Silva, J. Geophys. Res. **112**, B05206 (2007).
[31] Y. G. G. Yu and R. M. Wentzcovitch, J. Geophys. Res. **111**, B12202 (2006).
[32] Z. Wu and R. M. Wentzcovitch, J. Geophys. Res. **112**, B12202 (2007).
[33] Z. Q. Wu, R. M. Wentzcovitch, K. Umemoto, B. S. Li, K. Hirose, and J. C. Zheng, J. Geophys. Res. **113**, B06204 (2008).
[34] S. Grimme, J. Comput. Chem. **25**, 1463 (2004).
[35] S. Grimme, J. Comput. Chem. **27**, 1787 (2006).
[36] P. Giannozzi, S. Baroni, N. Bonini, M. Calandra, R. Car, C. Cavazzoni, D. Ceresoli, G. L. Chiarotti, M. Cococcioni, I. Dabo, A. Dal Corso, S. de Gironcoli, S. Fabris, G. Fratesi, R. Gebauer, U. Gerstmann, C. Gougoussis, A. Kokalj, M. Lazzeri, L. Martin-Samos, N. Marzari, F. Mauri,

R. Mazzarello, S. Paolini, A. Pasquarello, L. Paulatto, C. Sbraccia, S. Scandolo, G. Sclauzero, A. P. Seitsonen, A. Smogunov, P. Umari, and R. M. Wentzcovitch, J. Phys.: Condens. Matter **21**, 395502 (2009).
[37]P. Hohenberg and W. Kohn, Phys. Rev. B **136**, B864 (1964).
[38]W. Kohn and L. J. Sham, Phys. Rev. **140**, 1133 (1965).
[39]J. P. Perdew, K. Burke, and M. Ernzerhof, Phys. Rev. Lett. **77**, 3865 (1996).
[40]N. Troullier and J. L. Martins, Phys. Rev. B **43**, 1993 (1991).
[41]F. Shimojo, Z. Q. Wu, A. Nakano, R. K. Kalia, and P. Vashishta, J. Chem. Phys. **132**, 094106 (2010).
[42]R. M. Wentzcovitch, Phys. Rev. B **44**, 2358 (1991).
[43]F. Birch, Phys. Rev. **71**, 809 (1947).